Limnol. Oceanogr., 59(3), 2014, 1027–1034

doi:10.4319/lo.2014.59.3.1027

Ocean acidification enhances the growth rate of larger diatoms

Yaping Wu,[1,2,*] Douglas A. Campbell,[1] Andrew J. Irwin,[1] David J. Suggett,[3,a] and Zoe V. Finkel [1]

[1] Environmental Science, Mathematics & Computer Science, and Biology, Mount Allison University, Sackville, New Brunswick, Canada
[2] State Key Laboratory of Marine Environmental Science, Xiamen University, Xiamen, China
[3] School of Biological Sciences, University of Essex, Colchester, United Kingdom

Abstract

Ocean acidification is changing the nature of inorganic carbon availability in the global oceans. Diatoms account for ~ 40% of all marine primary productivity and are major contributors to the export of atmospheric carbon to the deep ocean. Larger diatoms are more likely to be stimulated by future increases in CO_2 availability as a result of their low surface area to volume ratio and lower diffusive flux of CO_2 relative to their carbon demand for growth. Here we quantify the effect of the partial pressure of carbon dioxide (P_{CO_2}), at levels of 190, 380, and 750 μL L^{-1}, on the growth rate, photosystem II electron transport rate (ETR), and elemental composition for five diatom species ranging over five orders of magnitude in cell volume. Growth rates for all species were enhanced under 750 relative to 190 and 380 μL L^{-1}, with little change in ETR or elemental stoichiometries, indicating an enhanced allocation of photochemical energy to growth under elevated P_{CO_2}. P_{CO_2} enhancement of growth rates was size dependent. Under 750 vs. 190 μL L^{-1} partial pressures, growth rate was enhanced by ~ 5% for the smaller diatom species to ~ 30% for the largest species examined. The size dependence of CO_2-stimulated growth enhancement indicates that ocean acidification may selectively favor an increase in the growth rates of larger vs. smaller phytoplankton species in the sea, with potentially significant consequences for carbon biochemistry.

Biomineralizing phytoplankton are significant contributors to the net annual atmospheric drawdown and burial of carbon in the global ocean (Fischer and Karakas 2009). Concerns have arisen over the potential effects of ocean acidification (OA) from anthropogenically induced increases to seawater partial pressure of carbon dioxide (P_{CO_2}) on the growth and biomineralization rates of marine phytoplankton (Riebesell et al. 2000; Finkel et al. 2010). Calcifying coccolithophores appear to be particularly affected, since OA both increases the availability of CO_2 for photosynthesis and decreases the availability of carbonate for calcification. The response of different coccolithophore species to OA appears to be highly variable (Riebesell et al. 1993, 2000; Iglesias-Rodriguez et al. 2008). Silicifying diatoms have received less attention since availability of silicate is not directly affected by OA; however, growing evidence suggests that OA may alter silicification (Milligan et al. 2004; Herve et al. 2012), growth rates, elemental composition, and productivity of marine diatoms (Burkhardt et al. 1999, 2001; Tortell et al. 2008).

Laboratory experiments simulating Intergovernmental Panel on Climate Change (IPCC) P_{CO_2} scenarios for 2100 have generally shown increased diatom growth rates compared to the present day (Burkhardt et al. 1999; Sun et al. 2011), but these increases can be subtle (Milligan et al. 2004; Li et al. 2012; Wu et al. 2012), in particular when other nutrients become limiting (Sun et al. 2011; Tatters et al. 2012). Some experiments have demonstrated that diatom growth can be negatively affected (Gao et al. 2012; Herve et al. 2012) by reduced pH and elevated P_{CO_2}, further highlighting that other factors, most notably light, can moderate the net response of diatom growth to ocean acidification. Field-based studies indicate that phytoplankton communities in both coastal and oceanic systems exposed to future projected increases in P_{CO_2} exhibit elevated diatom growth and, in some cases, enhanced phytoplankton community biomass (Tortell et al. 2008; Feng et al. 2009). As with the laboratory culturing experiments, such responses are by no means ubiquitous, but they clearly demonstrate the potential for diatoms to be positively influenced by ocean acidification when nutrients are replete and light is not inhibitory.

Evidence from across the various studies performed to date suggests that cell size could play a fundamental role as to whether (and how) diatoms ultimately respond to OA. Cell size directly determines CO_2 diffusion rate and whether the cell can meet its inorganic carbon requirements based on CO_2 diffusion alone (Wolf-Gladrow and Riebesell 1997). Under lower P_{CO_2}, CO_2 diffusion rates are less likely to meet the dissolved inorganic carbon (DIC) requirements for growth, especially for larger cells. Diatoms have carbon-concentrating mechanisms (CCMs) that facilitate the acquisition and concentration of DIC from the environment, including extracellular carbonic anhydrases that catalyze CO_2 influx into the cell by dehydrating HCO_3^- at the cell surface (Rost et al. 2003; Hopkinson et al. 2011). As a consequence, marine diatoms are unlikely to be strictly DIC growth limited in marine environments where HCO_3^- is available at high concentrations, but in cases where the physical rates of CO_2 diffusion do not meet the carbon demand of growth, an increase in P_{CO_2} may trigger a down regulation of the CCM and energetic savings that could stimulate increases in growth rate. Laboratory experiments have demonstrated that growth rates of larger as compared to smaller diatoms

* Corresponding author: yapingwu@xmu.edu.cn

[a] Present address: Plant Functional Biology and Climate Change Cluster, University of Technology, Sydney, Australia

appear to be more sensitive to increases in P_{CO_2} (Riebesell et al. 1993; Burkhardt et al. 1999). In the field, elevated P_{CO_2} has been shown to cause increases in diatom growth rate and a shift in the diatom-dominated community towards larger chain-forming and more heavily silicified species (Tortell et al. 2008). Larger biomineralized phytoplankton are associated with higher and more efficient rates of carbon export (Fischer and Karakas 2009). Consequently, if increases in P_{CO_2} stimulate increases in the growth rates of larger diatoms, resulting in disproportionate increases in the population sizes of larger diatoms, then OA may result in increases in the export of carbon to the deep ocean. We therefore sought to better understand how OA may alter the growth rate of diatoms of very different sizes. We examined how pre-industrial, current, and 2× current P_{CO_2} levels influence the photosystem II (PSII) electron transport rate (ETR), investment in Rubisco content, and elemental composition, as well as net growth rate, across five marine diatoms with cell volumes ranging over almost five orders of magnitude.

Methods

Species and culture conditions—Five centric diatom strains, *Thalassiosira pseudonana* (CCMP 1335), *Thalassiosira guillardii* (CCMP 988), *Thalassiosira weissflogii* (CCMP 1336), *Thalassiosira punctigera* (CCAP 1085/19), and *Coscinodiscus wailesii* (CCMP 2513), were acclimated to three different pH levels that correspond to P_{CO_2} levels of ~ 190, 380, and 750 μL L^{-1}. Culture strains were chosen to maximize the range of cell sizes and minimize phylogenetic differences. *Thalassiosira* species are bipolar centrics, and *C. wailesii* is a radial centric diatom. *Thalassiosira* may not be monophyletic, and different strains of *T. pseudonana* may belong to different clades (Kaczmarska et al. 2005). Culture vessels were completely filled with culture medium and sealed to avoid contact with air, kept optically thin at constant pH (*see* details below), and manually agitated four to five times every day. Cells were harvested after acclimation to different pH levels for at least eight cell divisions in midexponential phase. All species were grown in f/2 + Si media and maintained in midexponential growth phase using semicontinuous culture technique at 20°C in three to six replicate 1200 mL polycarbonate bottles illuminated with cool fluorescent tubes at a photon flux density of 350 μmol m^{-2} s^{-1} and a 12 : 12 light : dark cycle.

Media prepared with a total alkalinity of 2300 μmol kg^{-1} were enriched and then adjusted using HCl and $NaHCO_3$ (Gattuso et al. 2010) to pH 8.42 ± 0.03 (mean ± standard deviation [SD]), 8.16 ± 0.03, or 7.90 ± 0.03, corresponding to P_{CO_2} of 192 ± 15, 379 ± 30, and 747 ± 50 μL L^{-1}, respectively. To minimize effects of photosynthesis and respiration on the carbonate system, all cultures were maintained at maximum densities below 10 μg chlorophyll a (Chl *a*) L^{-1} by dilution with seawater medium, preadjusted to the target pH, in the middle of the light period. Culture pH was confirmed by regular measurements (AB15, Accumet). The concentration of dissolved inorganic carbon (DIC) was measured by filtering 0.5 mL of culture through a 0.22 μm filter into a closed glass vial, followed by acidification to release the DIC as CO_2 (McGinn et al. 2005), which was carried using a nitrogen air stream through an infrared gas analyzer (QuBit). A standard curve was established using a Na_2CO_3 solution at a series of known concentrations. P_{CO_2} was computed with CO2SYS software (Lewis and Wallace 1998) based on the known values of DIC, pH, salinity, and nutrients (Table 1). CO2SYS permits the use of different pH scales and performs the appropriate calibrations using the correct equilibrium constants.

Cell density, growth rate, and cell volume—Samples were taken from acclimated cultures and fixed with Lugol's solution. Species with diameters < 40 μm were counted with a Beckman Multisizer 3 Coulter Counter. Larger species were counted under the microscope using a Sedgwick Rafter chamber. The growth rate (μ d^{-1}) for each of the strains was determined by ordinary least squares linear regression of ln cell density (corrected for culture dilution) over time. Cell volume was estimated from linear dimensions from images taken with a camera attached to a light microscope calibrated with a micrometer, using Image-J software and assuming the cells are cylinders.

Pigment content and elemental composition—Chl *a* and *c* were estimated according to Ritchie (2006). Biogenic Si was estimated from 50 mL of culture filtered onto a 25 mm polycarbonate filter, washed with 20 mL of 3.4% NaCl, extracted in 4 mL of 0.2 mol L^{-1} NaOH solution at 80°C for 40 min, cooled, neutralized with 1 mL of 1 mol L^{-1} HCl, and then centrifuged at 5000 rotations per minute for 10 min. The Si concentration in the supernatant was measured colorimetrically using a spectrophotometer (Thermo GESYS20) following Mullin and Riley (1965). Carbon and nitrogen content of the cells was determined by filtering 100–200 mL of culture onto 13 mm precombusted (5 h at 450°C) GF/F filters, washed with 10 mL of 0.05 mol L^{-1} HCl to remove inorganic carbon, and dried at 45°C and stored in a desiccator before CN analysis (Vario ELIII, Elementar).

Rubisco and PSII content and ETR estimates—Rubisco and PSII protein contents were estimated using quantitative immunoblotting of RbcL and PsbA, respectively (Brown et al. 2008), by comparison to calibrated protein quantitation standards (AgriSera, AS03-037, AS01-017S, AS05-084, AS01-016S). The PSII electron transport rate (e- $PSII^{-1}$ s^{-1}) was estimated following Suggett et al. (2009) as:

$$\mathrm{ETR} = \mathrm{PFD} \times \sigma\mathrm{PSII}' \times q\mathrm{P} \times \mathrm{A} \quad (1)$$

where PFD is the photon flux (photon m^{-2} s^{-1}) measured with a Walz microspherical quantum sensor (Walz, Germany), σ_{PSII}' (m^2 $PSII^{-1}$) is the PSII effective absorption cross section for white light measured with a background actinic light and estimated by fast repetition rate fluorometry induction with a blue LED source (FIRe, Satlantic), corrected for the white growth light using a spectral correction factor for diatoms, $q\mathrm{P} = (F_M' - F_S) / (F_M' - F_0')$ (dimensionless) is

Table 1. The pH (National Bureau of Standards scale), DIC concentration, and the computed P_{CO_2} (μL L^{-1}), bicarbonate, carbonate, and CO_2 for each treatment and species. Data are the means ± SD of six measurements.

	P_{CO_2}	*T. pseudonana*	*T. guillardii*	*T. weissflogii*	*T. punctigera*	*C. wailesii*
pH	190	8.41±0.02	8.44±0.03	8.41±0.03	8.42±0.03	8.42±0.02
	380	8.20±0.02	8.17±0.04	8.17±0.02	8.19±0.03	8.19±0.03
	750	7.94±0.03	7.91±0.03	7.93±0.02	7.94±0.02	7.93±0.03
DIC (μmol kg^{-1})	190	1879±15	1872±22	1879±17	1874±31	1859±13
	380	2025±18	2030±18	2004±29	2040±16	2019±22
	750	2184±21	2150±18	2133±39	2165±22	2142±33
P_{CO_2} (μL L^{-1})	190	197±25	182±21	196±12	191±14	188±21
	380	363±34	386±41	387±31	372±40	371±48
	750	718±59	779±53	742±67	735±67	733±71
HCO_3^- (μmol kg^{-1})	190	1595±19	1574±17	1594±20	1585±16	1571±11
	380	1818±19	1833±12	1912±9	1834±11	1818±11
	750	2039±16	2013±15	1995±14	2021±14	2002±15
CO_3^{2-} (μmol kg^{-1})	190	278±9	292±18	278±21	183±17	282±12
	380	195±10	183±14	180±9	194±13	189±12
	750	122±7	111±7	113±6	119±6	116±7
CO_2 (μmol kg^{-1})	190	6.4±0.3	6.0±0.5	6.5±0.6	6.3±0.5	6.2±0.3
	380	11.9±0.8	12.9±1.1	12.9±0.8	12.2±1.0	12.3±1.0
	750	24.1±1.6	25.7±1.7	24.7±1.4	24.3±1.2	24.4±1.6

the approximate fraction of PSII open under the growth light level with F_M' and F_S extracted from the fluorescence rise profiles measured with a background level of actinic light, and F_0' approximated as F_0, and $A=1$ converts photons absorbed by PSII to electrons generated by PSII. To estimate PSII electron transport per cell, we multiplied by PSII content per cell, estimated as PsbD protein content measured with quantitative immunoblotting (Brown et al., 2008).

Data analyses—To determine if growth rate, ETR, or cellular content of carbon, nitrogen, phosphorous, silicate, chlorophyll, PSII, or Rubisco changed with P_{CO_2} treatment, we fit two models for each variable. The first model was an ordinary least squares regression of the $\log_{10}$ of the variable (X) against $\log_{10}$ cell volume, $\log X \sim \log_{10} a + b \log_{10} V$. The second model incorporated different intercepts and slopes for each P_{CO_2} treatment. We then compared the nested models with an F-test to determine if the models were different and thus if P_{CO_2} treatment had a significant effect. For each variable, we then performed type II major axis (MA) regression (Legendre 2013) to determine how each variable changed with cell volume and P_{CO_2} treatment. If the F-test showed there was a significant difference between P_{CO_2} treatments, we fit a model for each treatment; otherwise, we fit a single MA model for each variable. All analyses were preformed with R.

We estimated the carbon demand of growth relative to the supply by CO_2 diffusion. Carbon demand is the carbon requirement for doubling (C cell quota) over one generation. We calculated the diffusive flux of CO_2 to the cell surface in mol s^{-1} as

$$Q = 4\pi RD\left(1 + R\sqrt{\frac{k'}{D}}\right)\left([CO_2]_\infty - [CO_2]_r\right) \qquad (2)$$

where R is the equivalent cell radius estimated from cell volume, $D = 1.77 \times 10^{-5}$ cm^2 s^{-1}, and $k' = 0.018$ s^{-1} (Riebesell et al. 1993; Wolf-Gladrow and Riebesell 1997; Reinfelder 2011). $[CO_2]_\infty$ and $[CO_2]_r$ are the concentration of dissolved CO_2 in the bulk media and at the cell surface, respectively. $[CO_2]_\infty$ is estimated using CO2SYS, and we set $[CO_2]_r = (1/3) \times [CO_2]_\infty$ following Reinfelder (2011). This factor of 1/3 is a rough approximation, and the true value will likely vary with cell size and CO_2 treatment, but our overall conclusions are qualitatively unchanged for values of this ratio between 0.1 and 0.7. The CO_2 available by diffusion during a single generation is the product of this rate and the doubling time ($\ln 2/\mu$), multiplied by 1/2 to account for the 12 : 12 light : dark cycle. We incorporated a conservative discount to the C supply by dividing by 1.1 to account for 10% dark respiration.

Results

Cell diameters for the five species examined ranged from 2.5 to 180 μm. Mean cell volumes were 31 μm^3 for *T. pseudonana*, 534 μm^3 for *T. guillardii*, 4048 μm^3 for *T. weissflogii*, 54,670 μm^3 for *T. punctigera*, and 2,900,702 μm^3 for *C. wailesii*. There were only minor changes in cell volume within a species over the course of the experiment, and no significant effect of P_{CO_2} on cell volume was observed for the species examined (data not shown).

Growth rates of the five species ranged from 0.54 to 1.35 d^{-1} over all the P_{CO_2} treatments. The size-scaling exponent of growth rate, the slope of the major axis (MA) regression of $\log_{10}$ growth rate vs. $\log_{10}$ cell volume, increased significantly with increasing P_{CO_2} from −0.07 at 190, to −0.06 at 380, to −0.05 at 750 μL L^{-1} CO_2 (Fig. 1A; Table 1). A fertilization effect of CO_2 on growth rates was detected for all species; however, the CO_2 enhancement of growth rate increased with cell size, ranging from 5% up to 14% under 380 relative to 190 μL L^{-1} and ranging from 5% up to 33% under 750 relative to 190 μL L^{-1} P_{CO_2}. The largest CO_2 fertilization effect was observed for the two largest species under 750 relative to 190 μL L^{-1} (Fig. 1B), corresponding to treatments where CO_2 diffusion did not

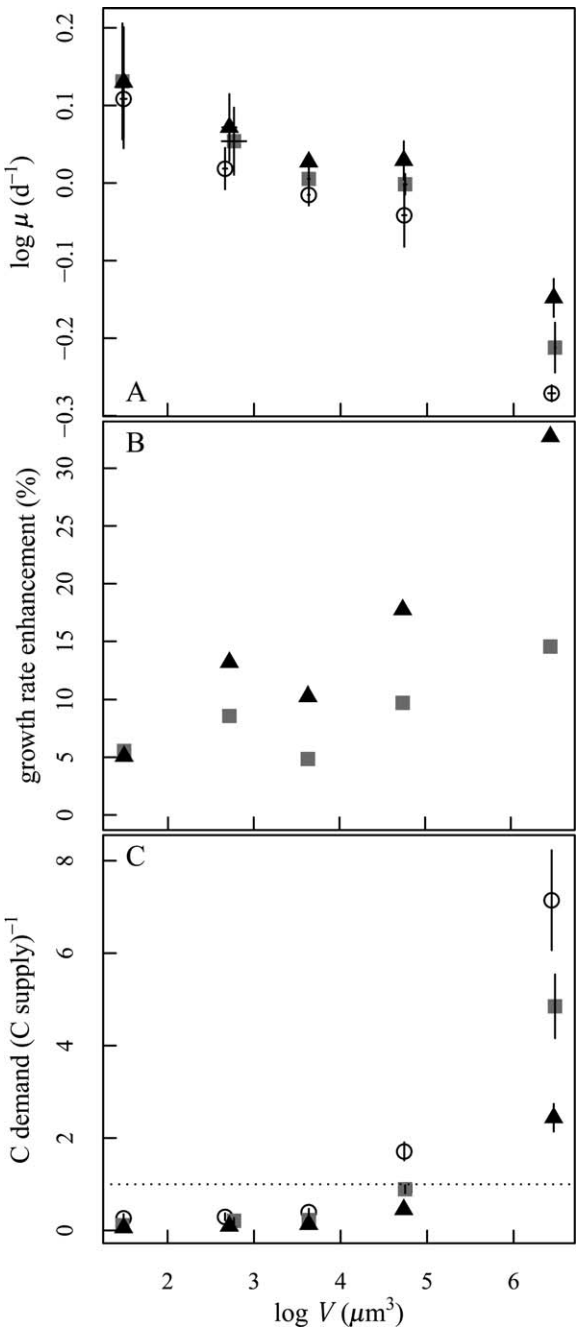

Fig. 1. (A) Log_{10} growth rate under 190, 380, and 750 μL L^{-1} P_{CO_2} as a function of log_{10} cell volume (V). (B) CO_2-stimulated growth rate enhancement at 380 μL L^{-1} (gray squares) or 750 μL L^{-1} (solid triangles) relative to 190 μL L^{-1}, as a function of log_{10} cell volume (V). (C) Carbon demand for growth relative to an estimate of CO_2 diffusion to the cell surface (see text), including conversion of HCO_3^- in the boundary layer assuming carbon losses were 10% of the growth demand as a function of log_{10} cell volume (V). Open circles, gray squares, and solid triangles represent 190, 380, and 750 μL L^{-1} P_{CO_2}. Vertical bars represent the 95% confidence intervals, n = 3–6. The horizontal dotted line represents a balance between demand and supply.

meet the net carbon demands associated with growth rate (Fig. 1C). For the three smallest *Thalassiosira* species, which experienced only a minor CO_2 fertilization effect, CO_2 diffusion exceeded the net carbon demands associated with growth rate (Fig. 1C). The largest species, *C. wailesii*, has a lower growth rate for its size than the *Thalassiosira* species and exhibited the largest changes with P_{CO_2} (Fig. 1A,B).

Cellular Chl *a* content ranged from 0.25 pg $cell^{-1}$ in the smallest species examined, *T. pseudonana*, to the highest value, 676 pg $cell^{-1}$, in the largest species examined, *C. wailesii* (Fig. 2). The size-scaling exponent (slope of MA regression for log_{10} Chl $cell^{-1}$ vs. log_{10} cell volume) for Chl *a* is 0.71, and P_{CO_2} had no significant effect on cellular chlorophyll concentration (Table 2) or the size-scaling exponent.

Log cellular carbon, nitrogen, silicon, Rubisco, and PSII content all increased with log cell volume, with size-scaling exponents ranging between 0.71 and 0.84, but as with Chl *a*, values did not vary significantly with P_{CO_2} (Fig. 2; Table 1). For some species, cellular Si quota decreased with increasing P_{CO_2}. C : Si was consistently higher under the highest P_{CO_2} treatment in the three smaller species but for the two larger species did not significantly vary over the range of P_{CO_2} examined. C : N (mol : mol) averaged 6.8 ($\pm$ 1.0 SD) across all species and treatments and did not vary consistently with P_{CO_2} across species.

PSII electron transport rates (e^{-1} s^{-1} μm^{-3}) scaled with cell volume, with a size-scaling exponent of -0.29, which again did not vary with P_{CO_2} (Table 2). As expected, larger cells had slower growth rates and slower cell volume–normalized ETRs; however, the growth rate achieved for a given ETR increased as P_{CO_2} increased, suggesting that proportionally more photochemical energy was invested into cell growth with increasing P_{CO_2}, particularly for the larger-sized species (Fig. 3).

Discussion

An increase in P_{CO_2} from 190 to 750 μL L^{-1} resulted in a 5% to 33% increase in diatom growth rate, with the largest CO_2 growth enhancement occurring in the largest diatom species, those having diameters in excess of 40 μm (Fig. 1). The small- to medium-sized diatom species, with diameters ranging from 4 to 30 μm, exhibited only minor, ~5%, changes in growth rate under P_{CO_2} ranging from 190 to 750 μL L^{-1}, consistent with previous work (Riebesell et al. 1993; Burkhardt et al. 1999; Li et al. 2012). As a consequence, the size-scaling exponents (cell volume) associated with diatom growth rates ($time^{-1}$) increased (became shallower) with increasing P_{CO_2} from 190 to 750 μL L^{-1} (Table 2). Consistent with previous studies, C : N and C : Si did not vary consistently with P_{CO_2} across species (Burkhardt and Riebesell 1997; Reinfelder 2012; Tatters et al. 2012). The results from this study indicate that increasing P_{CO_2} over the next century may result in a relative increase in the growth rates of large marine diatoms up to ~ 180 μm in diameter vs. smaller diatom species.

Can these experimental results from cultures be applied to diatoms living within a turbulent, well-mixed ocean? Estimates of the size of the smallest eddies and the

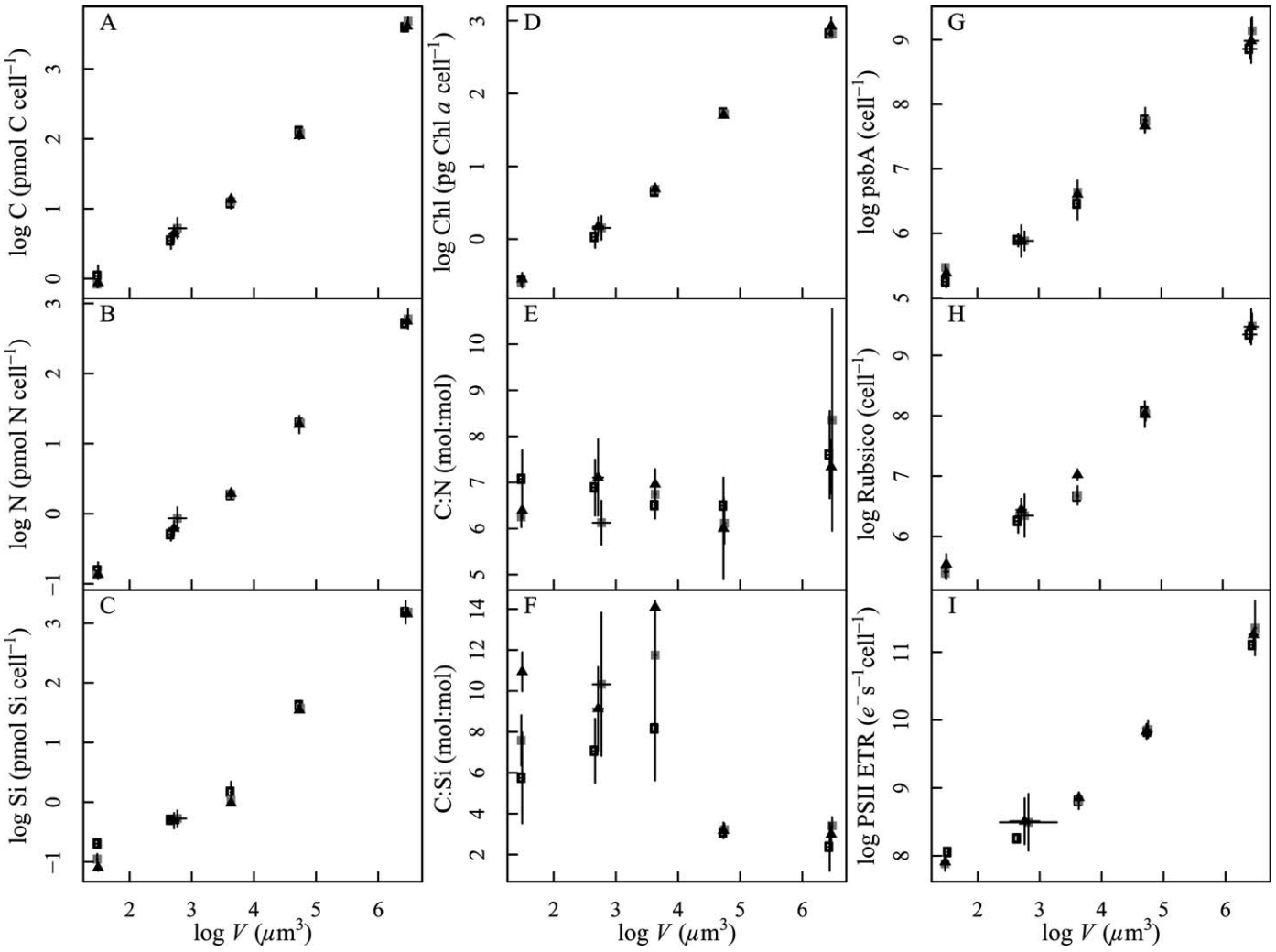

Fig. 2. The $\log_{10}$ (A) cellular carbon, (B) nitrogen, (C) silicon, and (D) chlorophyll *a*, and molar ratio of (E) C : N, (F) C : Si, and cellular (G) PSII, (H) Rubisco, and (I) PSII electron transport rate of the five species grown under 190, 380, and 750 μL L^{-1} P_{CO_2} as a function of $\log_{10}$ cell volume (V). Open circles, gray squares, and solid triangles represent 190, 380, and 750 μL L^{-1} P_{CO_2}. Vertical bars represent 95% confidence intervals, n = 3–6.

Sherwood number at high turbulent energies of 10^{-2} cm^2 s^{-3} indicate that cells less than 200 μm in diameter do not experience turbulent mixing in their immediate environment, and the enhancement of the transport of solutes, such as CO_2, to the cell surface relative to diffusion is very minor (Wolf-Gladrow and Riebesell 1997; Kiørboe 2008). Diatom species with diameters many hundreds to thousands of micrometers in diameter, such as *Ethmodiscus rex*, may have access to greater supply of CO_2 due to turbulence in the ocean, and therefore their growth response to increasing P_{CO_2} may be muted relative to cells $<$ 200 μm in diameter.

The potential for growth enhancement with increases in P_{CO_2} may be determined, at least in part, by the deficit between CO_2 supplied to the cell surface by diffusion and the carbon required for growth. The deficit between CO_2 supplied to the cell surface by diffusion and the carbon required for growth is size dependent, increasing with cell size and decreasing surface area to volume ratios (Fig. 1C). For diatom species with diameters less than 40 μm, under the experimental conditions investigated in this study, estimated rates of CO_2 diffusion, including the conversion of HCO_3^- to CO_2 in the nutrient-depleted zone around the cell surface, are well in excess of the carbon demand for net growth rate. In contrast, for diatoms with diameters greater than 40 μm, *T. punctigera* under 190 μL L^{-1} and *C. wailesii* under 190, 380, and 750 μL L^{-1} CO_2, the diffusive flux of CO_2 to the cell surface is not sufficient to meet the inorganic carbon demand required for the net growth rates obtained, assuming a conservative 10% carbon net loss to respiration (Fig. 1C). Increasing P_{CO_2} can reduce the deficit between CO_2 supplied to the cell surface by diffusion and the carbon required for growth. This may lead to a down regulation of the CCM and its associated costs, and a size-dependent enhancement of growth rate, as observed in this study. Smaller diatom species would also be expected to exhibit growth enhancement with increasing P_{CO_2} under conditions where carbon demand for growth is high, for

Table 2. The size-scaling (cell volume V, μm^3) intercept (a) and exponent (b) associated with each variable X (growth rate, photosystem II electron transport rate and cellular composition) from the model $\log X \sim \log_{10} a + b \log_{10} V$ together with their 95% confidence intervals (CI). r^2 and n refer to the data points used in the major axis regression estimate of the intercept (a) and size-scaling exponent (b) for each parameter. The F-statistic and p-value are reported for the analysis of variance for each parameter, testing if P_{CO_2} (μL L^{-1}) had a significant effect.

Variables X	P_{CO_2} (μL L^{-1})	Intercept a (95% CI)	Exponent b (95% CI)	r^2	n	F-value	p-value
μ (d^{-1})	190	0.23 (0.18, 0.28)	−0.071 (−0.08, −0.06)	0.90	15	6.32	<0.001
	380	0.24 (0.19, 0.29)	−0.064 (−0.08, −0.05)	0.90	15		
	750	0.22 (0.18, 0.26)	−0.052 (−0.06, −0.04)	0.88	15		
PSII ETR (e^- μm^3 s^{-1})	no P_{CO_2} effect	6.66 (6.52, 6.81)	−0.319 (−0.36, −0.28)	0.87	49	0.29	0.88
C $cell^{-1}$ (pmol)	no P_{CO_2} effect	−1.32 (−1.41, −1.24)	0.744 (0.72, 0.77)	0.98	81	0.16	0.96
N $cell^{-1}$ (pmol)	no P_{CO_2} effect	−2.11 (−2.19, −2.03)	0.734 (0.71, 0.76)	0.98	81	0.14	0.97
Si $cell^{-1}$ (pmol)	no P_{CO_2} effect	−2.44 (−2.58, −2.30)	0.839 (0.80, 0.88)	0.96	72	1.51	0.21
Chl *a* $cell^{-1}$ (pg)	no P_{CO_2} effect	−1.72 (−1.77, −1.66)	0.708 (0.69, 0.72)	0.99	81	0.73	0.57
Rubisco $cell^{-1}$ (No. particles)	no P_{CO_2} effect	4.15 (4.05, 4.25)	0.811 (0.78, 0.84)	0.98	71	1.57	0.19
PSII $cell^{-1}$ (No. particles)	no P_{CO_2} effect	−13.53 (−13.6, −13.4)	0.761 (0.73,0.79)	0.97	72	0.51	0.73

example, rapidly growing species (relative to their size) and toxin producers (Sun et al. 2011; Tatters et al. 2012).

Phytoplankton species can maintain growth rates with a carbon demand that exceeds the rate of CO_2 diffusion to the cell surface through a range of CCMs, including the catalyzed conversion of HCO_3^- to CO_2 inside and outside the cell by carbonic anhydrase and active uptake of HCO_3^- and CO_2 (Rost et al. 2003; Giordano et al. 2005). The CCMs used by diatoms to concentrate CO_2 at the site of carbon fixation are only partially characterized, but it has been hypothesized that the metabolic cost may be significant (Giordano et al. 2005; Hopkinson et al. 2011) and should decline with increasing P_{CO_2} (Hopkinson et al. 2011). A theoretical calculation estimates that a down

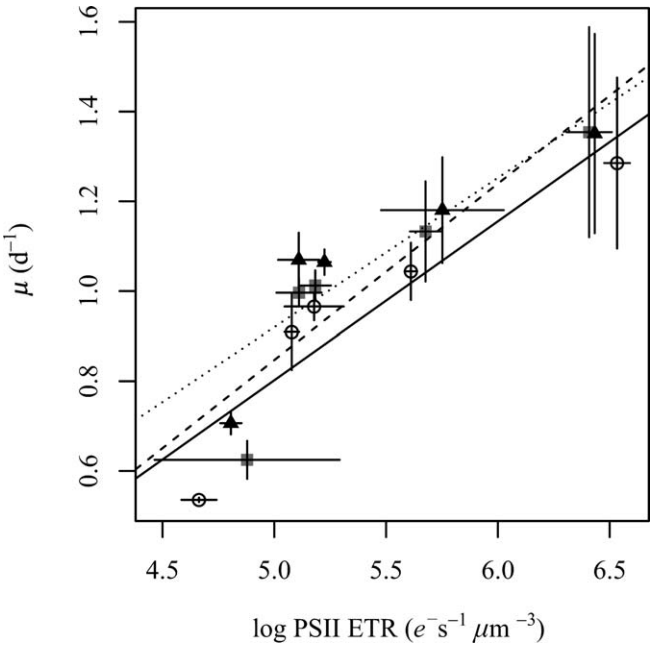

Fig. 3. Growth rate (d^{-1}) as a function of PSII electron transport rate ($\log_{10} e^-$ s^{-1} μm^{-3}). Open circles (solid line), gray squares (dashed line), and solid triangles (dotted line) represent 190, 380, and 750 μL L^{-1} P_{CO_2}. Vertical and horizontal bars represent 95% confidence intervals.

regulation of the CCM in response to a doubling of ambient CO_2 could increase carbon fixation rates in the small diatom *Phaeodactylum tricornutum* by 3–6% (Hopkinson et al. 2011). These predictions are consistent with our results for diatoms less than 40 μm in diameter whose growth rate demand for C is met by CO_2 diffusion and with the observed growth rate enhancement of *P. tricornutum* under elevated P_{CO_2} (Wu et al. 2012).

Access to energy ultimately constrains the ability of large marine phytoplankton to access enough carbon substrate via their CCMs to achieve maximum growth rates. Photosynthetic ETR per cell, PSII content, and Rubisco per cell did not vary significantly across P_{CO_2} treatments within species, indicating that light capture provided a similar amount of photosynthetically produced reductant for each of the diatom species under all three P_{CO_2} treatments (Table 2). Thus, the enhanced growth rate of the larger-sized diatom species under elevated P_{CO_2} must be achieved via a combination of increased diffusion rates and a lowering of metabolic costs, and it is likely due to the down regulation of active carbon acquisition (Rost et al. 2003; Brading et al. 2011). There may also be additional metabolic costs associated with growth under higher P_{CO_2} and lower pH, including maintenance of pH homeostasis and countering increased PSII repair costs associated with increased susceptibility to photo-inhibition (Gao et al. 2012; Li et al. 2012); however, larger diatom cells are less susceptible to photo-inactivation of PSII (Suggett et al. 2009; Key et al. 2010). Consequently, larger diatom species, and presumably larger-sized species of other phytoplankton groups, would generally appear to have an advantage over smaller-sized species under future OA scenarios.

Increasing CO_2 and other greenhouse gases are significantly altering atmospheric and ocean circulation and chemistry and are expected to affect phytoplankton primary production and community structure (Finkel et al. 2010). There is concern that future climate warming will lead to increased stratification and reduced nutrient concentrations, selecting for smaller phytoplankton cells, which dominate low-nutrient waters due to their low nutrient requirements and high nutrient uptake, resulting in global decreases in net primary and export production

(Bopp et al. 2005; Finkel et al. 2010). However, the potential effect of elevated P_{CO_2} has rarely been considered explicitly in biogeochemical models. Our results indicate that future increases in CO_2 would favor increased growth rates of larger diatoms, especially in productive regions, which may act to increase the rate and efficiency of carbon export from the surface to the deep sea, and hence help to offset reduced export though warming. Addressing how P_{CO_2}-induced changes in the size scaling of growth rate are further modified by interacting factors, such as warming, which should act to further increase cell metabolism and hence the demand for DIC, is an important next step.

Acknowledgments

Z.V.F., A.J.I., and D.A.C. were funded by the Natural Science and Engineering Research Council of Canada Discovery Program and the Canada Research Chair Program. D.J.S. was funded through the UK Natural Environmental Research Council's Ocean Acidification Research Program (NE/H017062/1). Y.W. was funded by the National Natural Science Foundation of China (41206091). We thank J. A. Jeans for assistance with protein immunoquantitations. We thank the anonymous reviewers for their suggestions, which improved the manuscript.

References

Bopp, L., O. Aumont, P. Cadule, S. Alvain, and M. Gehlen. 2005. Response of diatoms distribution to global warming and potential implications: A global model study. Geophys. Res. Lett. **32:** 1–4, doi:10.1029/2005GL023653

Brading, P., M. E. Warner, P. Davey, D. J. Smith, E. P. Achterberg, and D. J. Suggett. 2011. Differential effects of ocean acidification on growth and photosynthesis among phylotypes of *Symbiodinium* (Dinophyceae). Limnol. Oceanogr. **56:** 927–938, doi:10.4319/lo.2011.56.3.0927

Brown, C. M., J. D. MacKinnon, A. M. Cockshutt, T. A. Villareal, and D. A. Campbell. 2008. Flux capacities and acclimation costs in *Trichodesmium* from the Gulf of Mexico. Mar. Biol. **154:** 413–422, doi:10.1007/s00227-008-0933-z

Burkhardt, S., G. Amoroso, U. Riebesell, and D. Sültemeyer. 2001. CO_2 and HCO_3-uptake in marine diatoms acclimated to different CO_2 concentrations. Limnol. Oceanogr. **46:** 1378–1391, doi:10.4319/lo.2001.46.6.1378

———, and U. Riebesell. 1997. CO_2 availability affects elemental composition (C : N : P) of the marine diatom *Skeletonema costatum*. Mar. Ecol. Prog. Ser. **155:** 67–76, doi:10.3354/meps155067

———, I. Zondervan, and U. Riebesell. 1999. Effect of CO_2 concentration on C : N : P ratio in marine phytoplankton: A species comparison. Limnol. Oceanogr. **44:** 683–690, doi:10.4319/lo.1999.44.3.0683

Feng, Y., and others. 2009. The effects of increased pCO_2 and temperature on the North Atlantic spring bloom: I. The phytoplankton community and biogeochemical response. Mar. Ecol. Prog. Ser. **388:** 13–25, doi:10.3354/meps08133

Finkel, Z. V., J. Beardall, K. J. Flynn, A. Quigg, T. A. V. Rees, and J. A. Raven. 2010. Phytoplankton in a changing world: Cell size and elemental stoichiometry. J. Plankton Res. **32:** 119–137, doi:10.1093/plankt/fbp098

Fischer, G., and G. Karakas. 2009. Sinking rates and ballast composition of particles in the Atlantic Ocean: Implications for the organic carbon fluxes to the deep ocean. Biogeosciences **6:** 85–102, doi:10.5194/bg-6-85-2009

Gao, K., and others. 2012. Rising CO_2 and increased light exposure synergistically reduce marine primary productivity. Nature Clim. Change **2:** 519–523.

Gattuso, J.-P., K. Lee, B. Rost, and K. Schulz. 2010. Approaches and tools to manipulate the carbonate chemistry, p. 41–52. *In* U. Riebesell, V. J. Fabry, L. Hansson, and J.-P. Gattuso [eds.], Guide to best practices for ocean acidification research and data reporting. Publications Office of the European Union Luxembourg.

Giordano, M., J. Beardall, and J. A. Raven. 2005. CO_2 concentrating mechanisms in algae: Mechanisms, environmental modulation, and evolution. Annu. Rev. Plant Biol. **56:** 99–131, doi:10.1146/annurev.arplant.56.032604.144052

Herve, V., J. Derr, S. Douady, M. Quinet, L. Moisan, and P. J. Lopez. 2012. Multiparametric analyses reveal the pH-dependence of silicon biomineralization in diatoms. PLOS One **7:** e46722, doi:10.1371/journal.pone.0046722

Hopkinson, B., C. Dupont, A. Allen, and F. M. M. Morel. 2011. Efficiency of the CO_2-concentrating mechanism of diatoms. Proc. Nat. Acad. Sci. USA **108:** 3830–3837, doi:10.1073/pnas.1018062108

Iglesias-Rodriguez, and others. 2008. Phytoplankton calcification in a high-CO_2 world. Science **320:** 336–340, doi:10.1126/science.1154122

Kaczmarska, I., M. Beaton, A. C. Benoit, and L. K. Medlin. 2005. Molecular phylogeny of selected members of the order *Thalassiosirales* (Bacillariophyta) and evolution of the fultoportula. J. Phycol. **42:** 121–138, doi:10.1111/j.1529-8817.2006.00161.x

Key, T., A. McCarthy, D. A. Campbell, C. Six, S. Roy, and Z. V. Finkel. 2010. Cell size tradeoffs govern light exploitation strategies in marine phytoplankton. Environ. Microbiol. **12:** 95–104, doi:10.1111/j.1462-2920.2009.02046.x

Kiørboe, T. 2008. A mechanistic approach to plankton ecology. Princeton Univ. Press.

Legendre, P. 2013. lmodel2: Model II regression. R package version 1.7-1 [Internet]. Available from http://CRAN.R-project.org/package=lmodel2

Lewis, E., and D. Wallace. 1998. Program developed for CO_2 system calculations [Internet]. CDIAC. Available from http://cdiac.esd.ornl.gov/oceans/co2rprtnbk

Li, W., K. Gao, and J. Beardall. 2012. Interactive effects of ocean acidification and nitrogen-limitation on the diatom *Phaeodactylum tricornutum*. PLOS One **7:** e51590, doi:10.1371/journal.pone.0051590

McGinn, P. J., M. J. Jones, A. B. Macdonald, and D. A. Campbell. 2005. Light is required for low-CO_2 mediated induction of transcripts encoding components of the CO_2-concentrating mechanisms in the cyanobacterium *Synechococcus elongatus*: Analysis by quantitative reverse transcription-polymerase chain reaction (Q-RT-PCR). Can. J. Bot. **83:** 711–720, doi:10.1139/b05-055

Milligan, A. J., D. E. Varela, M. A. Brzezinski, and F. M. M. Morel. 2004. Dynamics of silicon metabolism and silicon isotope discrimination in a marine diatom as a function of pCO_2. Limnol. Oceanogr. **49:** 322–329, doi:10.4319/lo.2004.49.2.0322

Mullin, J. B., and J. P. Riley. 1965. The spectrophotometric determination of silicate-silicon in natural waters with special reference to seawater. Anal. Chim. Acta **46:** 491–501.

Reinfelder, J. R. 2011. Carbon concentrating mechanisms in eukaryotic marine phytoplankton. Annu. Rev. Mar. Sci. **3:** 291–315, doi:10.1146/annurev-marine-120709-142720

———. 2012. Carbon dioxide regulation of nitrogen and phosphorus in four species of mairne phytoplankton. Mar. Ecol. Prog. Ser. **466:** 57–67, doi:10.3354/meps09905

Riebesell, U., D. A. Wolf-Gladrow, and V. Smetacek. 1993. Carbon dioxide limitation of marine phytoplankton growth rates. Nature **361:** 249–251, doi:10.1038/361249a0

———, I. Zondervan, B. Rost, P. D. Tortell, R. E. Zeebe, and F. M. M. Morel. 2000. Reduced calcification of marine plankton in response to increased atmospheric CO_2. Nature **407:** 364–367, doi:10.1038/35030078

Ritchie, R. J. 2006. Consistent sets of spectrophotometric chlorophyll equations for acetone, methanol and ethanol solvents. Photosyn. Res. **89:** 27–41, doi:10.1007/s11120-006-9065-9

Rost, B., U. Riebesell, and S. Burkhardt. 2003. Carbon acquisition of bloom-forming marine phytoplankton. Limnol. Oceanogr. **48:** 55–67, doi:10.4319/lo.2003.48.1.0055

Suggett, D. J., C. M. Moore, A. E. Hickman, and R. J. Geider. 2009. Interpretation of fast repetition rate (FRR) fluorescence: Signatures of phytoplankton community structure versus physiological state. Mar. Ecol. Prog. Ser. **376:** 1–19, doi:10.3354/meps07830

Sun, J., D. A. Hutchins, Y. Feng, E. L. Seubert, D. A. Caron, and F.-X. Fu. 2011. Effects of changing pCO_2 and phosphate availability on domoic acid production and physiology of the marine harmful bloom diatom *Pseudo-nitzschia multi-series*. Limnol. Oceanogr. **56:** 829–840, doi:10.4319/lo.2011.56.3.0829

Tatters, A. O., F.-X. Fu, and D. A. Hutchins. 2012. High CO_2 and silicate limitation synergistically increase the toxicity of *Pseudo-nitzschia fraudulenta*. PLOS One **7:** e32116, doi:10.1371/journal.pone.0032116

Tortell, P. D., and others. 2008. CO_2 sensitivity of Southern Ocean phytoplankton. Geophys. Res. Lett. **35:** L04605, doi:10.1029/2007GL032583

Wolf-Gladrow, D., and U. Riebesell. 1997. Diffusion and reactions in the vicinity of plankton: A refined model for inorganic carbon transport. Mar. Chem. **59:** 17–34, doi:10.1016/S0304-4203(97)00069-8

Wu, X., G. Gao, M. Giordano, and K. Gao. 2012. Growth and photosynthesis of a diatom grown under elevated CO_2 in the presence of solar UV radiation. Fund. Appl. Limnol. **180:** 279–290, doi:10.1127/1863-9135/2012/0299

Associate editor: John Albert Raven

Received: 16 September 2013
Amended: 10 February 2014
Accepted: 03 March 2014